Inorganic Chemistry

Article

pubs.acs.org/IC

Thermal Hysteresis in a Spin-Crossover Fe^{III} Quinolylsalicylaldimine Complex, $Fe^{III}(5\text{-Br-qsal})_2Ni(dmit)_2\cdot solv$: Solvent Effects

Bruno J. C. Vieira, João C. Dias, Isabel C. Santos, Laura C. J. Pereira, Vasco da Gama, and João C. Waerenborgh*

Centro de Ciências e Tecnologias Nucleares, Instituto Superior Técnico, Universidade de Lisboa, 2695-066 Bobadela LRS, Portugal

Supporting Information

ABSTRACT: The Fe^{III} complexes $Fe(5\text{-Br-qsal})_2Ni(dmit)_2\cdot solv$ with solv = CH_2Cl_2 (**1**) and $(CH_3)_2CO$ (**2**) were synthesized, and their structural and magnetic properties were studied. While magnetization and Mössbauer spectroscopy data of **1** showed a gradual spin transition, compound **2** evidenced an abrupt transition with a thermal hysteresis of 13 K close to room temperature ($T_{1/2}\downarrow$ ~273 K and $T_{1/2}\uparrow$ ~286 K). A similar packing arrangement of segregated layers of cations and anions was found for **1** and **2**. In both low-spin, LS, structures there are a large number of short intra- and interchain contacts. This number is lower in the high-spin, HS, phases, particularly in the case of **1**. The significant loss of strong $\pi-\pi$ interactions in the cationic chains and short contacts in the anionic chains in the HS structure of **1** leads to alternating strong and weak bonds between cations along the cationic chains and the formation of unconnected dimers along the anionic chains. This is consistent with a significant weakening of the extended interactions in **1**. On the other hand, in the HS phase of **2** the 3D dimensionality of the short contacts observed in the LS phases is preserved. The effect of distinct solvent molecules on the intermolecular spacings explains the different spin crossover behaviors of the title compounds.

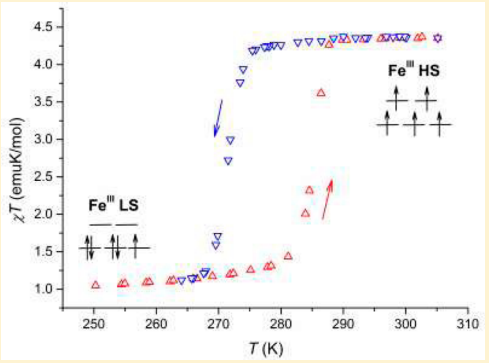

1. INTRODUCTION

Spin-crossover (SCO) complexes have drawn considerable attention for their potential applications as molecular devices. Since the SCO phenomenon may be induced by application of an external stimulus such as temperature, pressure, or light, introduction of such complexes as a building block in molecular materials is expected to confer a switching ability to the solid. The most studied systems have been based on Fe^{II}, but transition metal complexes of Fe^{III} with the coordination environment $Fe^{III}N_4O_2$ and with the advantage of being air stable also evidenced SCO behavior. This kind of transition is revealed by a magnetic and structural change and depends strongly on the cooperativity between building blocks.[1] Promoting this cooperativity by stronger intermolecular interactions established by bridging ligands, by hydrogen bonding, or by strong $\pi-\pi$ interactions has led to the observation of hysteresis in a number of SCO Fe^{II} compounds.[2] Although less common, hysteresis has also been reported for Fe^{III} SCO compounds.[3]

Many complexes based on $Fe(qsal)_2^+$ (Hqsal = *N*-(8-quinolyl)salicylaldimine)[3b,d,4,5] or on substituted qsal, $Fe(qnal)_2^+$ (Hqnal = *N*-(8-quinolyl)-2-hydroxy-1-naphthaldimine),[6] and $Fe(3\text{-}CH_3O\text{-}qsal)_2^+$[7] ligands, evidence a SCO phenomenon. Moreover, some of them, $Fe(5\text{-X-qsal})_2^+$ complexes with X = F, Cl, Br, I, OMe,[3c,f,g,i−k] evidenced hysteresis. In this paper we present the synthesis and characterization of two salts based on SCO Fe^{III} complexes of qsal-derived ligands and $Ni(dmit)_2$: $Fe(5\text{-Br-qsal})_2Ni(dmit)_2\cdot CH_2Cl_2$ (**1**) and $Fe(5\text{-Br-qsal})_2Ni(dmit)_2\cdot(CH_3)_2CO$ (**2**), where dmit = 4,5-dithiolato-1,3-dithiole-2-thione (Scheme 1). Both compounds have SCO transitions close to room temperature. One of them, **2**, shows a hysteresis of ~13 K.

2. EXPERIMENTAL DETAILS

2.1. Synthesis. Commercial solvents were used without further purification unless otherwise stated. The purity of the complexes and their solvation state was checked by determining the carbon, hydrogen, nitrogen, and sulfur content at the C²TN Elemental Analysis Service.

Scheme 1. Chemical Structures of $Fe(5\text{-Br-qsal})_2^+$ and $Ni(dmit)_2$

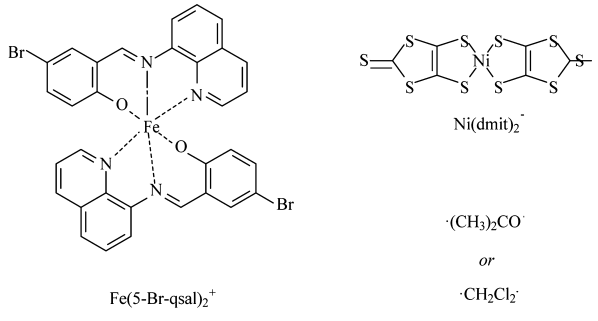

Received: September 18, 2014
Published: January 29, 2015

DOI: 10.1021/ic502278d
Inorg. Chem. 2015, 54, 1354−1362

Table 1. Crystallographic Data for Compounds 1 and 2 at 150 and 294 K

	1		2	
temp.	294 K	150 K	294 K	150 K
cryst size (mm)	0.29 × 0.21 × 0.12	0.20 × 0.10 × 0.08	0.16 × 0.10 × 0.08	0.28 × 0.08 × 0.05
cryst color, shape	black, prism	black, plate	black, plate	black, needle
empirical formula	$C_{39}H_{22}Br_2Cl_2FeN_4NiO_2S_{10}$	$C_{39}H_{22}Br_2Cl_2FeN_4NiO_2S_{10}$	$C_{41}H_{26}Br_2FeN_4NiO_3S_{10}$	$C_{41}H_{26}Br_2FeN_4NiO_3S_{10}$
mol. mass	1244.49	1244.49	1217.64	1217.64
wavelength (Å)	0.71069 (Mo Kα)	0.71069 (Mo Kα)	0.71069 (Mo Kα)	0.71069 (Mo Kα)
cryst syst	monoclinic	monoclinic	triclinic	triclinic
space group (no.)	$C2/c$ (15)	$C2/c$ (15)	$P\bar{1}$ (2)	$P\bar{1}$ (2)
a (Å)	23.5829(6)	23.414(1)	12.7802(8)	12.4127(5)
b (Å)	13.1228(4)	12.8049(6)	12.792(1)	12.5137(4)
c (Å)	30.5846(9)	30.690(1)	15.715(1)	16.1020(7)
α (deg)	90	90	71.671(2)	74.360(2)
β (deg)	109.463(1)	109.015(2)	82.983(2)	80.842(2)
γ (deg)	90	90	68.112(2)	68.142(3)
V (Å^3)	8924.3(4)	8699.3(7)	2262.9(3)	2230.5(2)
Z, Dc_{alcd} (Mg/m^3)	8, 1.852	8, 1.900	2, 1.787	2, 1.813
μ (mm^{-1})	3.168	3.250	3.009	3.053
F(000)	4944	4944	1216	1216
theta range (θ)	3.01−25.02	2.65−25.68	2.89−25.66	2.93−25.68
index range (h,k,l)	−28/28, −15/15, −36/36	−28/23, −15/15, −37/37	−15/15, −15/15, −19/19	−14/15, −15/15, −19/19
no. of reflns collected unique	29 081/7802 [R_{int} = 0.0505]	31 846/8241 [R_{int} = 0.0685]	14 868/8536 [R_{int} = 0.0465]	15 997/8440 [R_{int} = 0.0459]
T (max/min)	0.7423/0.4499	0.7810/0.5626	0.7948/0.6446	0.8623/0.4819
goodness-of-fit on F^2	1.053	1.049	0.909	0.920
Final $R1$, [$I > 2\sigma(I)$], $wR2$	0.0717, 0.1826	0.0589, 0.1361	0.0490, 0.0865	0.0456, 0.1003

Preparation of the Iron(III) Complex. $Fe^{III}(5\text{-Br-qsal})_2BPh_4$. In a glovebox, a mixture of 8-aminoquinoline, 144.2 mg (1 mmol), 5-bromo-salycilaldehyde, 201.0 mg (1 mmol), and 5 mL of methanol was refluxed for 4 h. After cooling to room temperature, solid sodium methoxide, 81.0 mg (1.5 mmol), was added and left reacting for a few minutes. Then, a solution of anhydrous $FeCl_3$, 81.1 mg (0.5 mmol), in 5 mL of methanol was added, and the mixture was left stirring overnight. After collection, the product was dried overnight with heating (304.0 mg). This solid was dissolved in 250 mL of hot methanol, the solution was filtered, and then a solution of $NaBPh_4$, 171.1 mg (0.5 mmol), in 2 mL of hot methanol was added dropwise. The mixture was left standing hot for ca. 30 min and then at room temperature overnight. The product was collected and dried with heating overnight. Yield: 261.9 mg (51%). Anal. Calcd (M_w = 1027.4): C, 65.46; H, 3.92; N, 5.45. Found: C, 65.47; H, 4.09; N, 5.39.

Preparation of Salts of Iron(III) Complexes with Nickel(III) Dithiolate. $Fe^{III}(5\text{-Br-qsal})_2Ni(dmit)_2{\cdot}CH_2Cl_2$ (1). In a glovebox, a filtered solution of TBA[Ni(dmit)$_2$], 146.0 mg (0.2 mmol), in 30 mL of hot dry dichloromethane was added slowly to a filtered solution of Fe^{III}(5-Br-qsal)$_2$BPh$_4$, 205.5 mg (0.2 mmol), in 150 mL of hot dry dichloromethane. The mixture was concentrated by heating for approximately 2 h to ca. 60 mL and then left standing at room temperature overnight. The precipitate was then collected. Yield: 133.0 mg (53%). Anal. Calcd for **1** (M_w = 1244.5): C, 37.64; H, 1.78; N, 4.50; S, 25.77. Found: C, 37.48; H, 1.89; N, 4.51; S, 25.01.

$Fe^{III}(5\text{-Br-qsal})_2Ni(dmit)_2{\cdot}(CH_3)_2CO$ (2). In a glovebox, a filtered solution of TBP Ni(dmit)$_2$, 109.0 mg (0.15 mmol), in 15 mL of hot dry acetone was added slowly to a filtered solution of Fe^{III}(5-Br-qsal)$_2$BPh$_4$, 154.1 mg (0.15 mmol), in 20 mL of hot dry acetone. The mixture was left standing with heating for ca. 30 min and then overnight at room temperature. The precipitate was collected and dried at air. Yield: 106.2 mg (58%). Anal. Calcd for **2** (M_w = 1217.7): C, 40.44; H, 2.15; N, 4.60; S, 26.33. Found: C, 40.73; H, 2.33; N, 4.20; S, 26.00.

2.2. X-ray Crystallography. A summary of the crystal data, experimental details, and refinement results are listed in Table 1, while selected bond distances and angles are presented in Table 2. The X-ray diffraction experiments were performed with a Bruker AXS APEX CCD detector four-circle diffractometer using a graphite-monochromated Mo Kα radiation source (λ = 0.71073 Å) in the ψ and ω scans mode. A semiempirical absorption correction was carried out using SADABS.[8] Data collection, cell refinement, and data reduction were done with the SMART and SAINT programs.[9] Structures were solved by direct methods using SIR97[10] and refined by full-matrix least-squares methods using the program SHELXL97[11] and a WINGX software package.[12] Non-hydrogen atoms were refined with anisotropic thermal parameters, whereas H atoms were placed in idealized positions and allowed to refine riding on the parent C atom. Molecular graphics were prepared using PLATON.[13]

2.3. Magnetic Characterization. Magnetic measurements were performed on a S700X SQUID magnetometer with a 7 T magnet (Cryogenic Ltd.) using polycrystalline samples. The temperature dependences of the magnetic susceptibility of **1** and **2** in the temperature range 5−320 K were measured under magnetic fields of 2 and 1 T, respectively. Measurements were performed in step mode. For each experimental point the temperature of the sample was equilibrated for at least 5 min. The paramagnetic susceptibility was obtained from the experimental magnetization data after diamagnetism corrections were estimated from the tabulated Pascal constants as -597.6×10^{-6} emu/mol for **1** and -835.0×10^{-6} emu/mol for **2**.

Mössbauer spectra were collected in the 295−77 K temperature range, in transmission mode, using a conventional constant-acceleration spectrometer and a 25 mCi ^{57}Co source in a Rh matrix. The velocity scale was calibrated using α-Fe foil. Isomer shifts are given relative to metallic α-Fe at 295 K. Disk-shaped absorbers were obtained by gently packing single crystals of each compound into perspex holders. Absorber thicknesses were calculated on the basis of the corresponding electronic mass-absorption coefficients for the 14.4 keV radiation, according to Long et al.[14] Low-temperature spectra were collected using a liquid-helium JANIS bath cryostat, model SVT-400, with the sample in He exchange gas. The spectra were fitted to Lorentzian lines using a nonlinear least-squares method.[15]

3. RESULTS AND DISCUSSION

3.1. Structural Characterization. Crystallographic data for **1** and **2** were collected on single crystals at 150 and 294 K (Table 1). Compound **1** crystallizes in the monoclinic space

DOI: 10.1021/ic502278d
Inorg. Chem. 2015, 54, 1354−1362

Table 2. Selected Bond Lengths [Angstroms] and Angles [degrees] for Compounds 1 and 2

	1		2	
	high temperature	low temperature	high temperature	low temperature
Fe1−O1	1.925(5)	1.881(4)	1.922(3)	1.903(3)
Fe1−O2	1.910(5)	1.882(4)	1.923(3)	1.898(3)
Fe1−N1	2.126(6)	1.947(5)	2.104(3)	1.962(4)
Fe1−N2	2.124(6)	1.987(5)	2.144(4)	1.986(4)
Fe1−N3	2.115(6)	1.964(5)	2.109(3)	1.955(4)
Fe1−N4	2.124(6)	1.984(5)	2.114(4)	1.973(4)
O1−Fe1−O2	95.4(2)	93.9(2)	96.8(1)	94.5(1)
O1−Fe1−N1	87.8(2)	94.5(2)	88.8(1)	94.8(2)
O2−Fe1−N1	100.8(2)	88.9(2)	97.0(1)	87.0(1)
O1−Fe1−N2	164.5(2)	176.1(2)	165.1(1)	175.9(2)
O2−Fe1−N2	90.0(2)	89.0(2)	90.2(1)	88.9(1)
N1−Fe1−N2	76.9(2)	82.9(2)	77.3(2)	82.9(2)
O1−Fe1−N4	91.1(2)	88.9(2)	87.1(1)	86.9(2)
O2−Fe1−N4	164.3(2)	176.1(2)	166.6(1)	177.4(2)
N1−Fe1−N4	93.7(2)	93.7(2)	95.9(1)	95.0(2)
N2−Fe1−N4	87.5(2)	88.4(2)	89.1(2)	89.8(2)
O1−Fe1−N3	99.0 (2)	88.1(2)	100.2(1)	88.3(1)
O2−Fe1−N3	87.9(2)	94.2(2)	89.4(1)	94.2(1)
N1−Fe1−N3	168.4(2)	175.8(2)	168.3(2)	176.6(2)
N2−Fe1−N3	95.7(2)	94.3(2)	92.9(1)	93.9(2)
N4−Fe1−N3	76.9(2)	83.1(2)	77.3(1)	83.7(2)

group $C2/c$, and its asymmetric unit contains one cation $[Fe^{III}(Br\text{-}qsal)_2]^+$, one anion $[Ni(dmit)_2]^-$, and one dichloromethane molecule.

Compound **2** crystallizes in the triclinic space group $P\bar{1}$ with an asymmetric unit comprising one cation, two half anions (nonequivalent), and one acetone molecule.

In **1** and **2**, at 150 K and room temperature, the coordination environment of the Fe^{III} centers in $[Fe^{III}(Br\text{-}qsal)_2]^+$ are distorted octahedra, with both deprotonated Br-qsal ligands oriented nearly perpendicular to each other, resulting in $Fe^{III}N_4O_2$ chromophores, where the coordinating O (and N_{imine}) atoms are cis relative to each other while the N_{amine} atoms are in a trans configuration.

The coordinating bond lengths and angles are summarized in Table 2. For both compounds at 150 K the Fe−O/N coordinating bond distances are comparable to those reported for other similar $[Fe(qsal)_2]^+$ cations in the low-spin, LS, state.[16] At room temperature those bonds are significantly longer for both compounds, by ∼0.04(0.02), ∼0.14(0.15), and ∼0.17(0.15) Å for Fe−X where X = O, N_{amine}, and N_{imine}, respectively (values in parentheses referring to compound **2**). Those distances are in good agreement with those reported for $[Fe(qsal)_2]^+$ cations in the high-spin, HS, state.[16] This expansion of the coordinating bond lengths is consistent with the occurrence of essentially complete SCO processes in both compounds as confirmed by the magnetic measurements and Mossbauer spectroscopy data (see below).

The octahedral distortion of this type of SCO Fe complexes and its correlation with the spin states have been evaluated on the basis of the parameters $\sum$ (quantifies the angular deviation from an ideal octahedral geometry) and Θ (indicates the distortion from an octahedral toward a trigonal prismatic geometry) .[3e] The parameters obtained for **1** at 150 and 294 K are $\sum$ = 41.3° and 68.6° and Θ = 60.8° and 203°, respectively. For **2** at the same temperatures those values are not much different, $\sum$ = 44.8° and 64.0° and Θ = 63.7° and 183°, respectively. The lower values of the parameters at 150 K are consistent with the existence of a stronger ligand field, indicating a LS state for both **1** and **2**, while the higher values at room temperature indicate a HS state.

The crystal structure of **1** is based on the arrangement of alternating cationic and anionic layers parallel to the *ab* plane, with the solvent molecules included within the anionic layers. A view of the crystal structure of **1** obtained at 150 K along [110] is shown in Figure 1. The cationic layers are composed of parallel chains of $[Fe(Br\text{-}qsal)_2]^+$ cations with the chains alternating along the [110] and [1$\bar{1}$0] directions in neighboring cationic layers. Within those chains the cations present strong $\pi-\pi$ contacts between the large aromatic fragments of the Br-qsal ligands.

Hereafter interatomic distances lower than the sum of the van der Waals radii, as defined by Bondi,[17] will be considered short contacts (Table S2, Supporting Information). A partial view of a cationic layer at 150 K is shown in Figure 2. In Figure S1, Supporting Information, two distinct overlapping modes between Br-qsal ligands may be observed: A and B. Similar overlapping modes along the cationic chains have been observed and described in detail for other $[Fe^{III}(X\text{-}qsal)_2]^+$ (X = halogen, OMe) based complexes.[3f,g,j,k]

For the LS structure of **1** the distance between the average mean planes of the Br-qsal ligands is 3.274 Å in the A mode, while in the B mode it is 3.450 Å (Table S1, Supporting Information). Furthermore, in the A mode 10 short $\pi-\pi$ contacts (3.242−3.396 Å) are observed between a pair of $[Fe^{III}(Br\text{-}qsal)_2]^+$ molecules, while the B mode only involves 3 short $\pi-\pi$ contacts (3.251−3.375 Å) between one cation of this pair and a third $[Fe^{III}(Br\text{-}qsal)_2]^+$ cation belonging to another cation pair of the same cation chain, as shown in Figure S1 and Tables S1 and S2, Supporting Information. A few weaker C−H (2.719 Å) and Br−H (3.000 Å) connections are observed between the cations from neighboring chains within the same cationic layer.

The anionic layers consist of an arrangement of parallel 1D zigzag chains running along [110] or [1$\bar{1}$0] based on the repetition of two nearly perpendicular $[Ni(dmit_2)]^-$ anions that present short S−S contacts (3.394 Å) through the peripheral S atoms of the dmit ligands (Figure 3). The arrangement of this pair of anions then propagates on the layers through contacts either along [110] or [1$\bar{1}$0] of one of the S from the C_2S_2C ring with a S in the terminal C═S group from the neighboring anions. These contacts (3.588 Å) are however very close to the sum of the Bondi radii and may be only van der Waals contacts. Short cation−anion S−H (2.722−2.939 Å) and S−C (3.444−3.451 Å) contacts are observed between every cation and anion located on the anionic layers above and below the cationic layer ("above" and "below" defined along the *c* direction in Figure 1)

DOI: 10.1021/ic502278d
Inorg. Chem. 2015, 54, 1354−1362

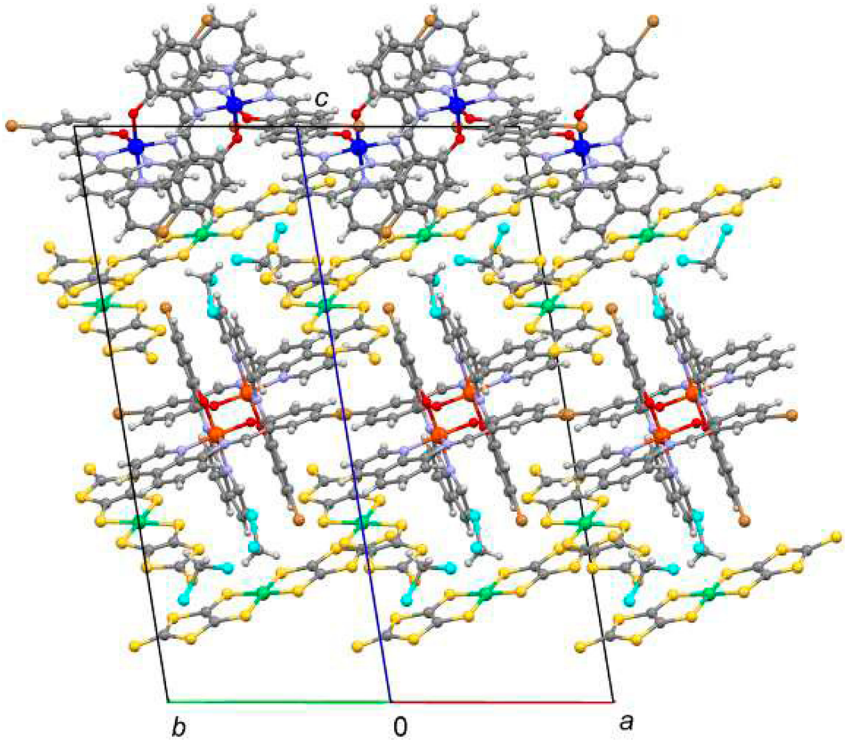

Figure 1. View of the crystal structure of compound **1** along [110] (at 150 K), showing two cationic and two anionic layers.

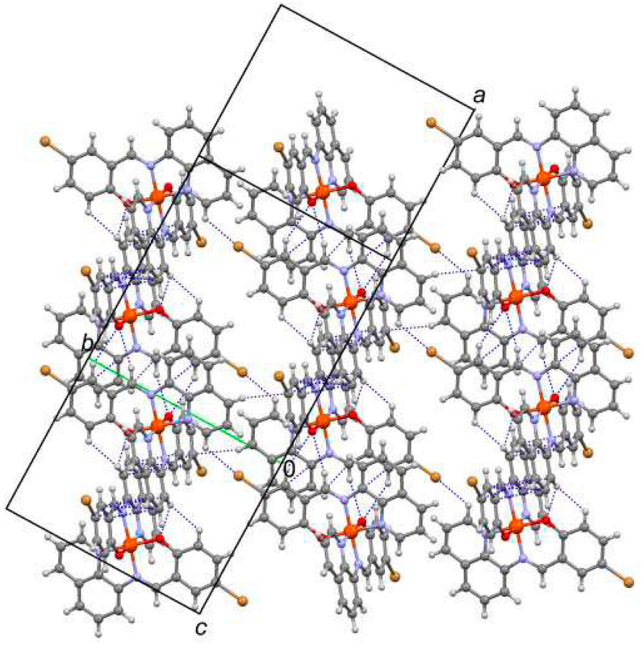

Figure 2. Cationic layer of **1** at 150 K showing the strong $\pi-\pi$ contacts between the large aromatic fragments of the Br-qsal ligands. Short contacts are shown as dark blue dashed lines.

providing a 3D connectivity between the anionic and the cationic 2D networks.

The solvent molecules form pairs included in cavities within the anionic 2D network (Figure 3). The estimated Cl−Cl distances of 2.909 Å between CH_2Cl_2 molecules within those pairs are abnormally low. The atomic displacement parameters observed for these Cl atoms are very high (0.2−0.5 $Å^3$), suggesting positional disorder. This disorder on the Cl sites may explain the physically impossible interatomic Cl−Cl distance.

A variety of anion−solvent S−H (2.895−2.933 Å) and cation−solvent Cl−H (2.788−2.823 Å) and Cl−C (3.351 Å) contacts contribute to the 3D connectivity between the anionic and the cationic 2D networks.

The crystal structure of the LS phase of **2** is also based on an alternating layered network of cations and anions. Figure 4 shows a view of the crystal structure of **2** at 150 K along [010]. The cationic layers consist of an arrangement of parallel chains of cations along [010]. A view of a cationic layer at 150 K is shown in Figure 5. In these chains strong $\pi-\pi$ contacts are observed through the large aromatic fragments of the Br-qsal ligands. The same A and B overlapping modes between Br-qsal ligands referred to above for **1** may be observed in the LS structure of **2** involving four (3.284−3.347 Å) and three (3.312−3.327 Å) short $\pi-\pi$ contacts (Figure S2 and Table S2, Supporting Information). The distance between the average mean planes of the Br-qsal ligands is 3.316 and 3.362 Å for the A and B overlapping modes, respectively (Table S1, Supporting Information). The acetone molecules are located in voids within the cationic layers and reinforce the intrachain contacts through short O−H contacts (2.491 and 2.672 Å) between the solvent molecules and the neighboring cations in the same chain.

The anionic layers are composed of parallel chains of $[Ni(dmit_2)]^-$ anions, aligned along [100]. A view of an anionic layer, at 150 K, is shown in Figure 6. Strong S−S intrachain contacts (3.416 Å between S2 and S6, and three others varying between 3.511 and 3.546 Å) are observed, while distinct chains are relatively isolated from each other, no short interchain contacts being observed. In **2** there are neither cation−cation nor anion−anion interchain contacts. However, every cation has strong S−H (2.863 Å), S−C (3.456 Å), Ni−H (2.794 Å), and Ni−Br (3.442 Å) bonds to anions on both surrounding

DOI: 10.1021/ic502278d
Inorg. Chem. 2015, 54, 1354−1362

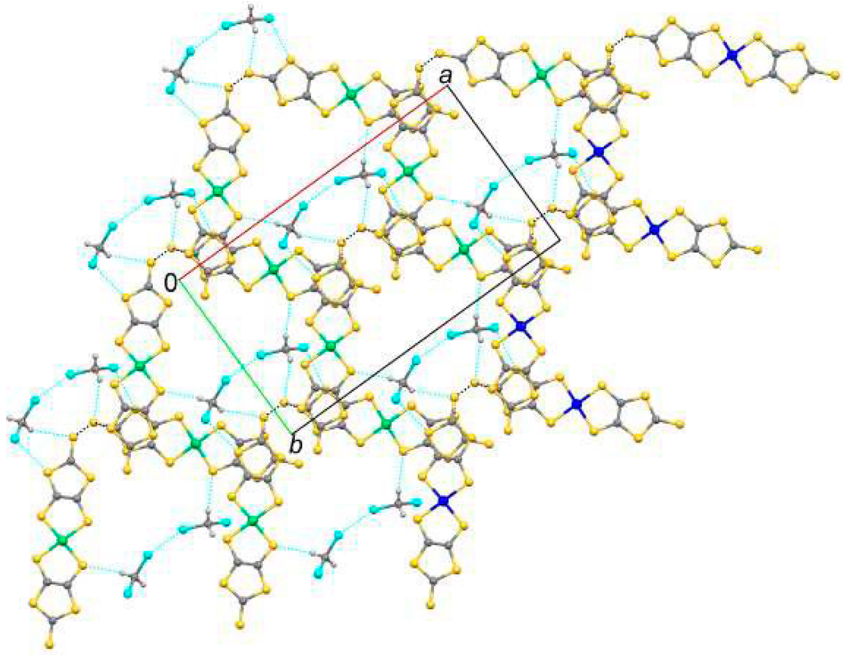

Figure 3. Anionic layer of **1** at 150 K showing the short contacts between anions (dark blue) and between anions and solvent molecules (light blue).

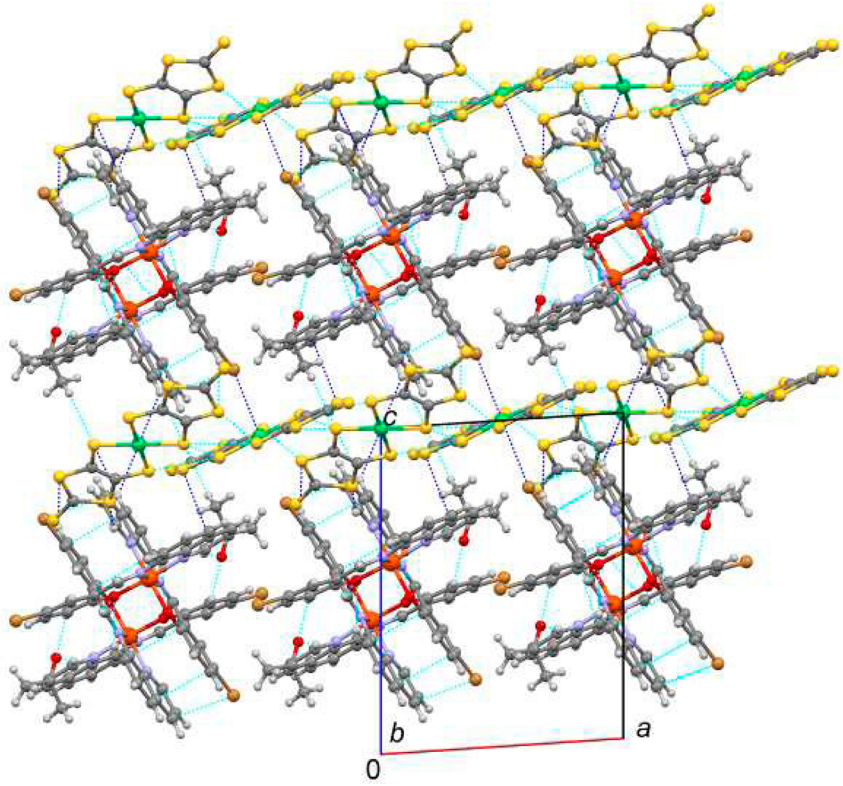

Figure 4. View of the crystal structure of **2** along [010] at 150 K, showing two cationic and two anionic layers. Dashed lines represent the short contacts, the darker ones corresponding to the interlayer cation−anion contacts.

anion layers (Figure 4). These bonds together with anion−solvent S−H (2.827 Å) short contacts provide connectivity between the isolated cationic and anionic chains leading to 3D connectivity.

For both **1** and **2**, apart from the intramolecular thermal expansion of the $[Fe(Br\text{-}qsal)_2]^+$ cations associated with the LS ↔ HS transformation, the overall packing of cation and anion molecules is essentially maintained in the corresponding LS and HS phases.

The SCO process and the induced variation in the Fe^{III} octahedral distortion in **1** leads to a significant increase of the distance between the average mean planes of the Br-qsal ligands, from 3.274 to 3.363 Å and from 3.450 to 3.562 Å in the A and B overlapping modes, respectively (Table S1, Supporting

DOI: 10.1021/ic502278d
Inorg. Chem. 2015, 54, 1354−1362

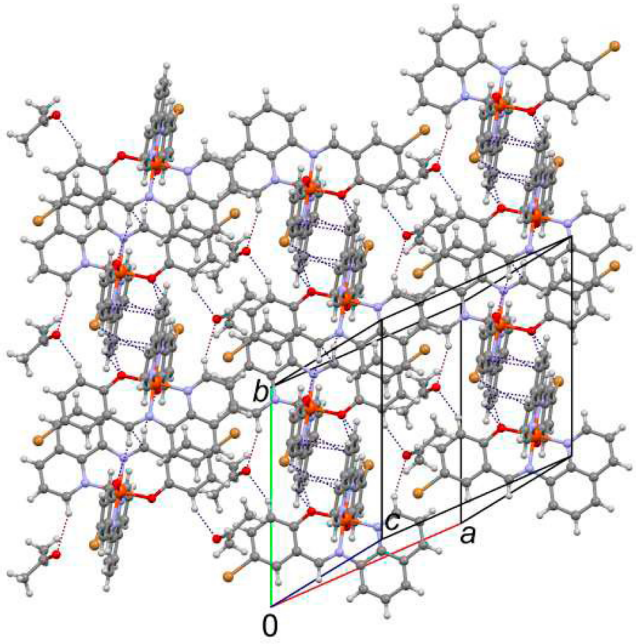

Figure 5. Cationic layers of **2** at 150 K showing the short contacts as dashed lines.

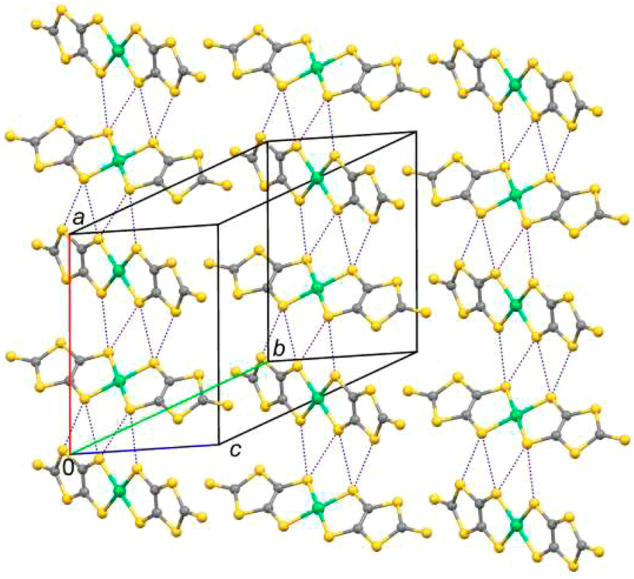

Figure 6. Anionic layers of **2** at 150 K showing the short contacts as dashed lines.

Information). The number of short C−C contacts decrease and interatomic distances of the remaining ones also increase for both overlapping modes from 3.242 to 3.349 Å and from 3.251 to 3.339 Å (Table S2, Supporting Information). The weaker C−H and Br−H contacts between chains within the same cationic layer are also elongated up to 2.886 and 3.041 Å, respectively, close to the sum of the van der Waals radii.

In **2** the general structural variation in the cationic sublattice associated with the SCO process is essentially similar to the situation described for **1**. However, a significant difference is found between both cases: in the HS phase of **2** the distance between the average mean planes of the Br-qsal ligands increases for the A and B overlapping modes 0.035 and 0.045 Å, much less than in **1** where the increase is 0.089 and 0.112 Å, respectively. In particular, in the HS phase of **2** this distance for the B overlapping mode, 3.407 Å, becomes much shorter than 3.562 Å in the HS phase of **1** (Figures S1 and S2 and Tables S1 and S2, Supporting Information). Stronger $\pi-\pi$ interactions, keeping the extended connectivity throughout the cationic chain, are therefore expected in **2**, while in **1** significantly weakened bonds are found between every pair of cations within a cationic chain.

Important differences are also observed between the anionic sublattices of **1** and **2**. In **1** the short S−S contacts between pairs of anions are present in both the LS and the HS phases (3.394 and 3.405 Å, respectively), but the connectivity in the HS phase is weakened through a significant increase (from 3.588 Å up to well above the sum of the van der Waals radii, 3.688 Å) in the contacts of the S from the C_2S_2C ring with a S in the terminal C═S group from the neighboring anion.

Unconnected pairs of anions are thus formed. In **2**, although an increase in the S−S interanionic distances (from 3.416 to 3.499 Å) slightly weakens the intrachain interactions between anions in the HS phase, the connectivity is still maintained along the anionic chains.

The rearrangement of the cation−anion contacts in **1** observed upon the LS → HS transition leads to a significant increase of several bonds but also to the shortening of a few others S−H (2.707 Å) and S−Br (3.590 Å). Short contacts are maintained in the HS phase between the cations and the anions on layers above and below the cationic layer (defining above and below along *c* in Figure 1). However, this connectivity is not expected to be efficient in the propagation of the structural distortion associated with the SCO phenomenon due to the above referred breaking of short contacts between anion pairs and weak bonds between cation pairs within cationic chains.

In **2**, the transition to the HS phase also decreases the number of anion−cation strong bonds. The remaining short contact, Ni−H, is shortened from 2.794 to 2.725 Å and a new one, S−H (2.921 Å), appears. In the LS phase each cation is bonded to anions on both surrounding layers located above and below the cationic layer, along *c* (Figure 4). In the HS phase each cation only bonds to one of the surrounding anion layers. However, the next cation on the same chain is linked to the alternative surrounding anion layer, i.e., while one cation links to the anion layer below, the next one links to the anion layer above. Considering the intrachain bonds between every pair of cations and anions within the cationic and anionic chains the above referred anion−cation contacts are expected to preserve the 3D connectivity through the lattice of the HS phase.

In the LS phase of **1** there are two H−Cl contacts (2.788 and 2.823 Å) between the cations and the dichloromethane molecules, where the Cl atom from the solvent establishes a weak bridge between two cations, but after the SCO transition only the shortest of these contacts is found considerably elongated up to 2.914 Å. In the LS phase of **2** an acetone molecule bridges two cations within the cationic chains through two O−H contacts (2.491 and 2.670 Å). In the HS phase a small readjustment of the positioning of the solvent molecule and of the cations is observed, and only the shortest of those contacts is kept although stretched out to 2.611 Å.

The contacts established by the solvent molecules are however less important for the 3D connectivity than the stronger $\pi-\pi$ interactions. As referred to above in the LS → HS transition a more significant weakening of the intrachain $\pi-\pi$ cation−cation interactions occurs in **1** when compared to **2** considering the higher distance between the average mean

DOI: 10.1021/ic502278d
Inorg. Chem. 2015, 54, 1354−1362

planes of the Br-qsal ligands in **1**. The formation of unconnected anion pairs in the HS phase of **1** further contributes to a weakening of the 3D net of short contacts in this compound, while in the HS phase of **2** intrachain bonds are preserved between every pair of anions. The anion−cation interchain interactions are thus able to keep the 3D connectivity in the HS phase of **2**. The effective propagation of the communication throughout the lattice of **2** is thus expected to lead to a significant cooperativity of the SCO phenomena in this compound.

3.2. Magnetic Characterization. The thermal dependence of χT, where χ is the paramagnetic susceptibility and T the absolute temperature, of **1** and **2** is presented in Figure 7. In

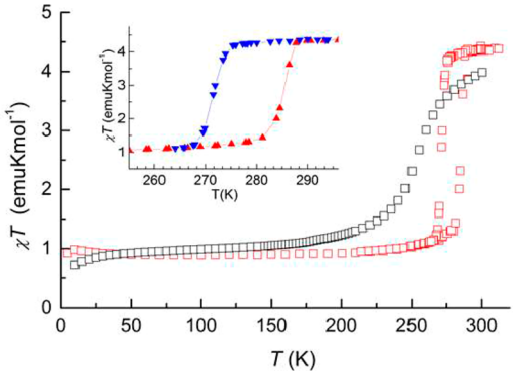

Figure 7. Thermal dependence of χT for **1** and **2** (black and red squares, respectively). (Inset) Detailed view of the χT behavior of **2** at high temperatures (blue and red triangles corresponding to cooling and warming branches).

these compounds the magnetic susceptibility is expected to be the sum of the contributions of the anionic and cationic sublattices (χ_A and χ_C, respectively), based on the $S = 1/2$ $[Ni(dmit)_2]^-$ anions and on the $S = 1/2$ (LS) or S = 5/2 (HS) $[Fe(Br\text{-}qsal)_2]^+$ cations

$$\chi = \chi_c + \chi_A \tag{1}$$

At low temperatures χT is nearly constant with a value of the order of 0.9 emu·K·mol^{-1}, which is consistent with $S = 1/2$ $[Ni(dmit)_2]^-$ and $S = 1/2$ $[Fe(Br\text{-}qsal)_2]^+$ networks. The drastic increase of χT, at high temperatures, indicates the existence of SCO processes for both compounds. While in the case of **2** a clear hysteresis of ∼13 K and a sharp SCO transformation is observed, in the case of **1** the process seems to be gradual and no significant hysteresis is detected. The results further indicate that for **2** at room temperature the SCO process is complete. χT saturates at 4.35 emu·K·mol^{-1}. Calculated spin-only values for $S = 5/2$ and $1/2$ are 4.475 and 0.375 emu·K·mol^{-1}. The measured χT value for $S = 1/2$ $[Ni(dmit)_2]^-$ at 300 K is however 0.33 emu·K·mol^{-1} (ref 3i). The experimental value of 4.36 emu·K·mol^{-1} observed for compound **2** is thus consistent with a contribution from Fe^{III} of 4.03 emu·K·mol^{-1}. This value is not equal to the calculated $S = 5/2$ spin-only value, but it is within the range of reported experimental values for Fe^{III} complexes, namely, $[Fe(qsal)_2]^+$ and $[Fe(X\text{-}qsal)_2]^+$ complexes, where all the Fe^{III} is in the HS state.[3b,d,i−k] For **1** at room temperature $\chi T = 4.0$ emu·K·mol^{-1} is still increasing, indicating that the SCO process is not yet complete.

The anion−anion interactions mediated by the short S−S contacts in the crystal structure of **1** and **2** suggest the existence of significant magnetic interactions between the $S = 1/2$ $[Ni(dmit)_2]^-$ anions. Most of the spin density on the cations is located at the Fe^{III} central atoms, and the contacts in the periphery of the ligands are not expected to lead to significant magnetic interactions. This is confirmed by the constant value of χT consistently observed in compounds containing this type of cations.[18] For the same reason the anion−cation magnetic interactions, which involve mostly the H atoms from the periphery of the Br-qsal ligands, are also expected to be rather weak and will be ignored. The contribution of the cationic sublattice to the magnetic susceptibility, χ, of these compounds is described by

$$\chi_c = f\chi^{HS} + (1 - f)\chi^{LS} \tag{2}$$

where f and $1 - f$ are the fractions of the HS and LS Fe atoms, respectively. χ^{HS} and χ^{LS} (the limit values of χ_C for $f = 1$ and 0) are given by the Curie Law[19]

$$\chi^{iS} = \frac{N_A\mu_B{}^2}{3kT} g_{is}{}^2 S_{is}(S_{is} - 1) \tag{3}$$

where N_A is Avogadro's number, g is the g factor of the species iS (iS = LS, with $S = 1/2$, or iS = HS with $S = 5/2$), μ_B is the Bohr magneton, and k is the Boltzmann constant.

At low temperatures ($T < 100$ K and $T < 150$ K for **1** and **2**, respectively), the SCO processes seem to be completed and the HS fraction $f = 0$. In these temperature ranges χ is the result of the sum of χ^{LS} with the contribution of the anion networks of **1** and **2** (χ_A), which may be described by a Curie−Weiss law[20]

$$\chi_A = \frac{N_A\mu_B{}^2}{3k(T - \theta)} g_A{}^2 S_A(S_A - 1) \tag{4}$$

where θ accounts for the anion−anion (AA) interactions. Equations 1−4 were used to describe the behavior of **1** and **2** at low temperatures with $f = 0$, $S_C = S_A = 1/2$. The fits to the experimental results of **1** are well fitted with $g_C = 2.40$, $g_A = 2.08$, $\theta = -14.7$ K, and a temperature-independent paramagnetism[19a] TIP = 7×10^{-4} emu·mol^{-1}, while for compound **2**, $g_C = 2.26$, $g_A = 2.08$, and $\theta = 2.1$ K were obtained (the detail of the fits are shown in Figure S3, Supporting Information). The θ values obtained indicate that in compound **1** the magnetic behavior from the anionic sublattice is dominated by significant antiferromagnetic (AFM) AA interactions, while for compound **2** the results are consistent with dominant weak ferromagnetic (FM) AA interactions. Although for compounds based on $[Ni(dmit)_2]^-$ dominant AFM interactions are the most frequent situation, there are a few cases where the dominant AA interactions were observed to be FM.[21] This may be attributed to a spin polarization effect in the $S = 1/2$ $[Ni(dmit)_2]^-$ anions.[21] Depending on the particular inter-anionic overlap the competition between AFM and FM contacts may lead to the predominance of either AFM or FM interactions as discussed in detail for some nickel bisdithiolene-based salts.[22]

The Mössbauer spectra obtained below 230 K for **1** consist of single-quadrupole doublets (Figure 8). The relative areas of both peaks in each doublet are not equal, very likely due to texture effects. These effects are expected since crystals used to prepare the Mössbauer absorber have a particular cleavage that should give rise to preferred orientation effects after packing.

All remaining spectra of **1** taken from 250 K to room temperature may be fitted with two quadrupole doublets. The

DOI: 10.1021/ic502278d
Inorg. Chem. 2015, 54, 1354−1362

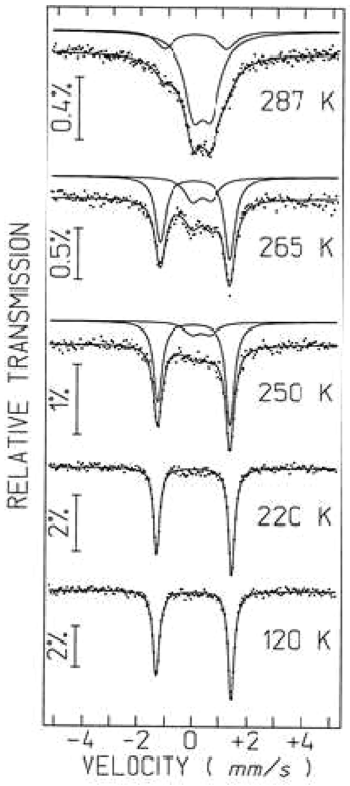

Figure 8. Mössbauer spectra of **1** taken at different temperatures.

estimated parameters (Table S3, Supporting Information) for the doublet with lower splitting are typical of HS Fe^{III}. The larger quadrupole splitting QS and lower IS estimated for the remaining doublet in each spectrum are expected LS Fe^{III}. The relative areas of the HS Fe^{III} increase with increasing temperature up to 287 K. The broad lines of HS Fe^{III} may be explained by relaxation effects. Due to the negligible magnetic orbital moment of Fe^{III} with $S = 5/2$, its paramagnetic relaxation time should be much lower than that of LS Fe^{III}.[23]

The spectra of **2** taken at 295 K and below 260 K are consistent with all Fe^{III} in the HS state and all Fe^{III} in the LS state, respectively (Figure 9). The spectra taken between 270 and 285 K depend however on the thermal history of the sample. If the spectrum is taken at 278 K after cooling from room temperature all of the Fe^{III} remains HS. It is necessary to further cool to 273 K to observe the conversion of more than one-half of the Fe^{III} to the LS state. After converting all of the Fe^{III} to the LS state at 260 K it remains in the same LS state even after heating up to 275 K. It is necessary to further increase the temperature to 285 K to convert ca. one-quarter of the Fe^{III} to the HS state. Finally, at 292 K all of the Fe^{III} is in the HS state again. These results are in agreement with the hysteresis observed in magnetization data. They further show that the metastable states of Fe^{III} both in the upward (~285 K) and in the downward (~273 K) branches of the hysteresis loop are kept for at least ~4 days, the time necessary to accumulate each Mössbauer spectra.

4. CONCLUSIONS

A similar packing of segregated layers of cations and anions is observed for compounds **1** and **2**. The presence of different solvent molecules, however, leads to different intermolecular spacings and distinct SCO behaviors. In the LS phases of both

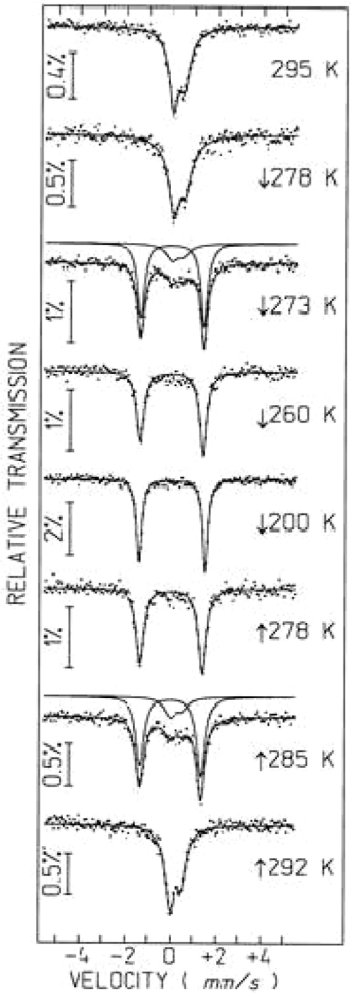

Figure 9. Mössbauer spectra of **2** taken at different temperatures.

compounds a large number of $\pi-\pi$ interactions between Fe(5-Br-qsal)$^+$ cations and short contacts between Ni(dmit)$^-$ anions are observed. Short cation−anion and cation−solvent contacts provide a 3D connectivity between the anionic and the cationic 2D networks. In the HS phases their number is reduced. However, while in the HS phase of **1** the 3D dimensionality of the short contacts is severely weakened, in the HS phase of **2** the extended connectivities throughout the cationic and anionic chains observed in the LS phases are preserved.

The different short contact arrangements in the HS phases play a crucial role in the SCO behavior exhibited by each compound. In **2** a more rigid lattice responds to the SCO structural deformation, while in **1** a softer lattice is involved. Compound **1** shows a gradual SCO transition taking place in a wide temperature range and no thermal hysteresis. On the other hand, compound **2** undergoes an abrupt, complete SCO and shows a thermal hysteresis with a promising value of 13 K, very close to room temperature ($T_{1/2}\downarrow$ ~273 K and $T_{1/2}\uparrow$ ~ 286 K). This feature is a strong motivation to explore the effect of different solvent molecules on the Fe(5-Br-qsal)$_2$Ni(dmit)$_2$ complexes.

A final note concerning the anions of **1** and **2**, dithiolene anions are often used in SCO compounds in order to explore a possible connection between the SCO and the conductivity of the material.[3i,6b] The conductivity of **1** and **2** was measured, but both compounds turned out to be insulators.

DOI: 10.1021/ic502278d
Inorg. Chem. 2015, 54, 1354−1362

■ ASSOCIATED CONTENT

Supporting Information

Additional figures and tables (including details from Mössbauer and crystallographic data). This material is available free of charge via the Internet at http://pubs.acs.org. CCDC reference numbers 1015937 (**1** at 150 K), 1015938 (**1** at 294 K), CCDC 1015939 (**2** at 150 K), and 1015940 (**2** at 294 K).

■ AUTHOR INFORMATION

Corresponding Author

*Phone: +351-21 994 6220. Fax: +351-21 955 0117. E-mail: jcarlos@ctn.ist.utl.pt.

Notes

The authors declare no competing financial interest.

■ ACKNOWLEDGMENTS

This work was partially supported by Fundação para a Ciência e Tecnologia (Portugal) under contracts PTDC/QUI/65379/2006 and RECI/QEQ-QIN/0189/2012 and grant SFRH/BPD/21873/2005. This work also benefited from the MAGMANet network of excellence.

■ REFERENCES

(1) (a) Kahn, O.; Martinez, C. *J. Science* **1998**, *279*, 44−48. (b) Gütlich, P. *Eur. J. Inorg. Chem.* **2013**, 581−591.

(2) (a) Kröber, J.; Codjovi, E.; Kahn, O.; Groliére, F.; Jay, C. *J. Am. Chem. Soc.* **1993**, *115*, 9810−9811. (b) Létard, J.-F.; Guionneau, P.; Codjovi, E.; Lavastre, O.; Bravic, G.; Chasseau, D.; Kahn, O. *J. Am. Chem. Soc.* **1997**, *119*, 10861−10862. (c) Zhong, Z. J.; Tao, J.-Q.; Yu, Z.; Dun, C.-Y.; Lui, Y.-J.; You, X.-Z. *J. Chem. Soc., Dalton Trans.* **1998**, 327−328. (d) Galet, A.; Munoz, M. C.; Gaspar, A. B.; Real, J. A. *Inorg. Chem.* **2005**, *44*, 8749−8755. (e) Hagiwara, H.; Hashimoto, S.; Matsumoto, N.; Iijima, S. *Inorg. Chem.* **2007**, *46*, 3136−3143. (f) Fujinami, T.; Nishi, K.; Matsumoto, N.; Iijima, S.; Halcrow, M. A.; Sunatsuki, Y.; Kojima, M. *Dalton Trans.* **2011**, *40*, 12301−12309. (g) Nishi, N.; Kondo, H.; Fujinami, T.; Matsumoto, N.; Iijima, S.; Halcrow, M. A.; Sunatsuki, Y.; Kojima, M. *Eur. J. Inorg. Chem.* **2013**, 927−933. (h) Nowak, R.; Bauer, W.; Ossiander, T.; Weber, B. *Eur. J. Inorg. Chem.* **2013**, 975−983.

(3) (a) Haddad, M. S.; Federer, W. D.; Lynch, M. W.; Hendrickson, D. N. *Inorg. Chem.* **1981**, *20*, 131−139. (b) Hayami, S.; Gu, Z.-Z.; Yoshiki, H.; Fujishima, A.; Sato, O. *J. Am. Chem. Soc.* **2001**, *123*, 11644−11650. (c) Dorbes, S.; Valade, L.; Real, J. A.; Faulmann, C. *Chem. Commun.* **2005**, 69−71. (d) Hayami, S.; Hiki, K.; Kawahara, T.; Maeda, Y.; Urakami, D.; Inoue, K.; Ohama, M.; Kawata, S.; Sato, O. *Chem.—Eur. J.* **2009**, *15*, 3497−3508. (e) Halcrow, M. A. *Chem. Soc. Rev.* **2011**, *40*, 4119−4142. (f) Harding, D. J.; Sertphon, D.; Harding, P.; Murray, K. S.; Moubaraki, B.; Cashion, J. D.; Adams, H. *Chem.—Eur. J.* **2013**, *19*, 1082−1090. (g) Harding, D. J.; Phonsri, W.; Harding, P.; Gass, I. A.; Murray, K. S.; Moubaraki, B.; Cashion, J. D.; Liud, D. J.; Telferd, S. G. *Chem. Commun.* **2013**, *49*, 6340−6342. (h) Fujinami, T.; Koike, M.; Matsumoto, N.; Sunatsuki, Y.; Okasawa, A.; Kojima, M. *Inorg. Chem.* **2014**, *53*, 2254−2259. (i) Fukuroi, K.; Takahashi, K.; Mochida, T.; Sakurai, T.; Ohta, H.; Yamamoto, T.; Einaga, Y.; Mori, T. *Angew. Chem., Int. Ed.* **2014**, *53*, 1983−1986. (j) Phonsri, W.; Harding, D. J.; Harding, P.; Murray, K. S.; Moubaraki, B.; Gass, I. A.; Cashion, J. D.; Jameson, G. N. L.; Adams, H. *Dalton Trans.* **2014**, *43*, 17509−17518. (k) Harding, D. J.; Phonsri, W.; Harding, P.; Murray, K. S.; Moubaraki, B.; Jameson, G. N. L. *Dalton Trans.* **2015**, in press; 10.1039/c4dt03184a.

(4) Nihei, M.; Shiga, T.; Maeda, Y.; Oshio, H. *Coord. Chem. Rev.* **2007**, *251*, 2606−2621.

(5) Dias, J. C.; Soriano-Portillo, A.; Clemente-Léon, M.; Giménez-Saiz, C.; Galán-Mascarós, J. R.; Gómez-García, C. J.; Coronado, E. *Inorg. Chim. Acta* **2007**, *360*, 3843−3847.

(6) (a) Zelentsov, V. V. *Russ. J. Coord. Chem.* **1998**, *24*, 295−299. (b) Takahashi, K.; Cui, H.; Okano, Y.; Kobayashi, H.; Mori, H.; Tajima, H.; Einaga, Y.; Sato, O. *J. Am. Chem. Soc.* **2008**, *130*, 6688−6689.

(7) Dias, J. C.; Vieira, B.; Santos, I. C.; Pereira, L. C. J.; Gama, V. *Inorg. Chim. Acta* **2009**, *362*, 2076−2079.

(8) Sheldrick, G.M. *SADABS*; Bruker AXS Inc.: Madison, WI, 2004.

(9) *SMART and SAINT*; Bruker AXS Inc.: Madison, WI, 2004.

(10) Altomare, A.; Burla, M. C.; Camalli, M.; Cascarano, G.; Giacovazzo, G.; Guagliardi, A.; Moliterni, A. G. G.; Polidori, G.; Spagna, R. *J. Appl. Crystallogr.* **1999**, *32*, 115−119.

(11) Sheldrick, G.M. *SHELXL97, Program for Crystal Structure Refinement*; University of Göttingen: Göttingen, Germany, 1997.

(12) Farrugia, L. J. *J. Appl. Crystallogr.* **1999**, *32*, 837−838.

(13) Farrugia, L. J. *J. Appl. Crystallogr.* **1997**, *30*, 565−565.

(14) Long, G. J.; Cranshaw, T. E.; Longworth, G. *Mossbauer Effect Ref. Data J.* **1983**, *6*, 42−49.

(15) Waerenborgh, J. C.; Salamakha, P.; Sologub, O.; Gonçalves, A. P.; Cardoso, C.; Sério, S.; Godinho, M.; Almeida, M. *Chem. Mater.* **2000**, *12*, 1743−1749.

(16) Sertphon, D.; Harding, D. J.; Harding, P.; Murray, K. S.; Moubaraki, B.; Cashion, J. D.; Adams, H. *Eur. J. Inorg. Chem.* **2013**, *2013*, 788−795.

(17) (a) Bondi, A. *J. Phys. Chem.* **1964**, *68*, 441−451. (b) Rowland, R. S.; Taylor, R. *J. Phys. Chem.* **1964**, *100*, 7384−7391.

(18) Vieira, B. J. C.; Coutinho, J. T.; Santos, I. C.; Pereira, L. C. J.; Waerenborgh, J. C.; Gama, V. *Inorg. Chem.* **2013**, *52*, 3845−3850.

(19) (a) Carlin, R. L. *Magnetochemistry*; Springer-Verlag: Berlin, 1986; pp 10−18. (b) Kahn, O. *Molecular Magnetism*; VCH Publishers, Inc. Ltd.: New York, 1993.

(20) McConnell, H. M. *J. Chem. Phys.* **1963**, *39*, 1910−1910.

(21) Faulmann, C.; Rivière, E.; Dorbes, S.; Senocq, F.; Coronado, E.; Cassoux, P. *Eur. J. Inorg. Chem.* **2003**, 2880−2888.

(22) (a) Fourmigué, M. In *Conducting and Magnetic Organometallic Molecular Materials*; Fourmigué, M., Ouahab, L., Eds.; Springer: Berlin, Heidelberg, 2009; Vol. *27*, pp 161−189. (b) Valade, L.; Faulmann, C. In *Conducting and Magnetic Organometallic Molecular Materials*; Fourmigué, M., Ouahab, L., Eds.; Springer: Berlin, Heidelberg, 2009; Vol. *27*, pp 141−159. (c) Belo, D.; Figueira, M. J.; Nunes, J. P. M.; Santos, I. C.; Pereira, L. C.; Gama, V.; Almeida, M.; Rovira, C. *J. Mater. Chem.* **2006**, *16*, 2746−2756.

(23) (a) Timken, M. D.; Abdel-Mawgoud, A. M.; Hendrickson, D. N. *Inorg. Chem.* **1986**, *25*, 160−164. (b) Clemente-Léon, M.; Coronado, E.; López-Jordá, M.; Mínguez Espallargas, G.; Soriano-Portillo, A.; Waerenborgh, J. C. *Chem.—Eur. J.* **2010**, *16*, 2207−2219. (c) Griffin, M.; Shakespeare, S.; Shepherd, H. J.; Harding, C. J.; Létard, J.-F.; Desplanches, C.; Goeta, A. E.; Howard, J. A. K.; Powell, A. K.; Mereacre, V.; Garcia, Y.; Naik, A. D.; Muller-Bunz, H.; Morgan, G. G. *Angew. Chem., Int. Ed.* **2011**, *50*, 896−900.

DOI: 10.1021/ic502278d
Inorg. Chem. 2015, 54, 1354−1362